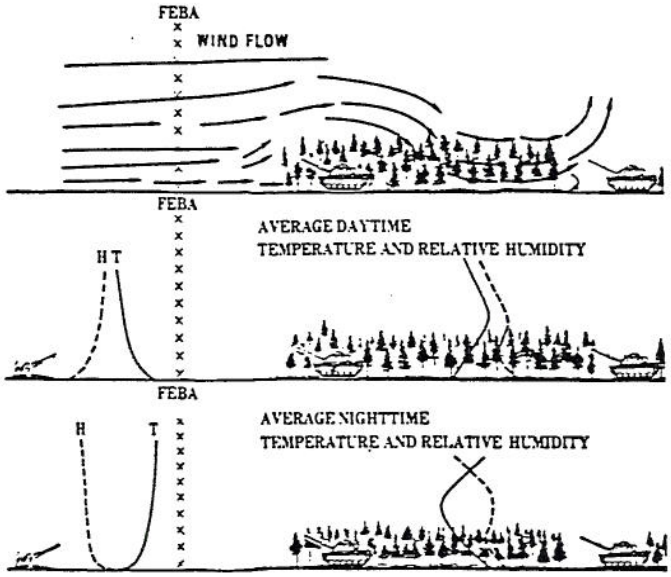


**Figure 3.4.1** Windflow and vertical profiles of meteorological variables within and above a forest. (Cionco, 1982)

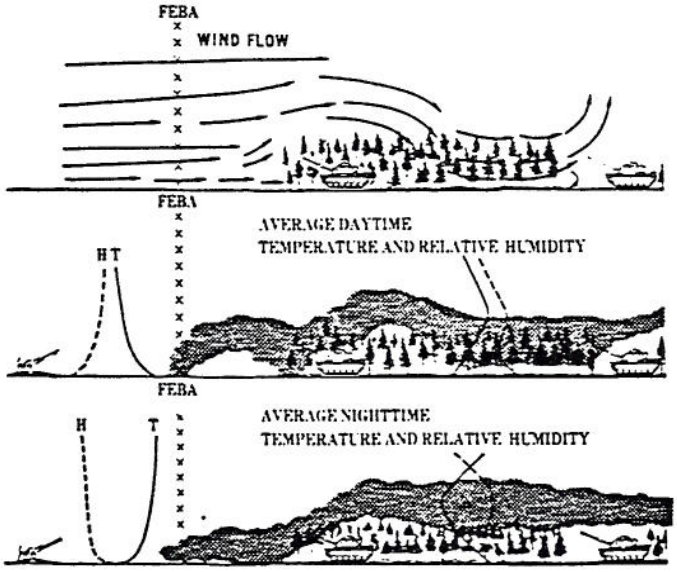


**Figure 3.4.2** Figure 3.4.1 with smoke plumes deployed. (Cionco, 1982)

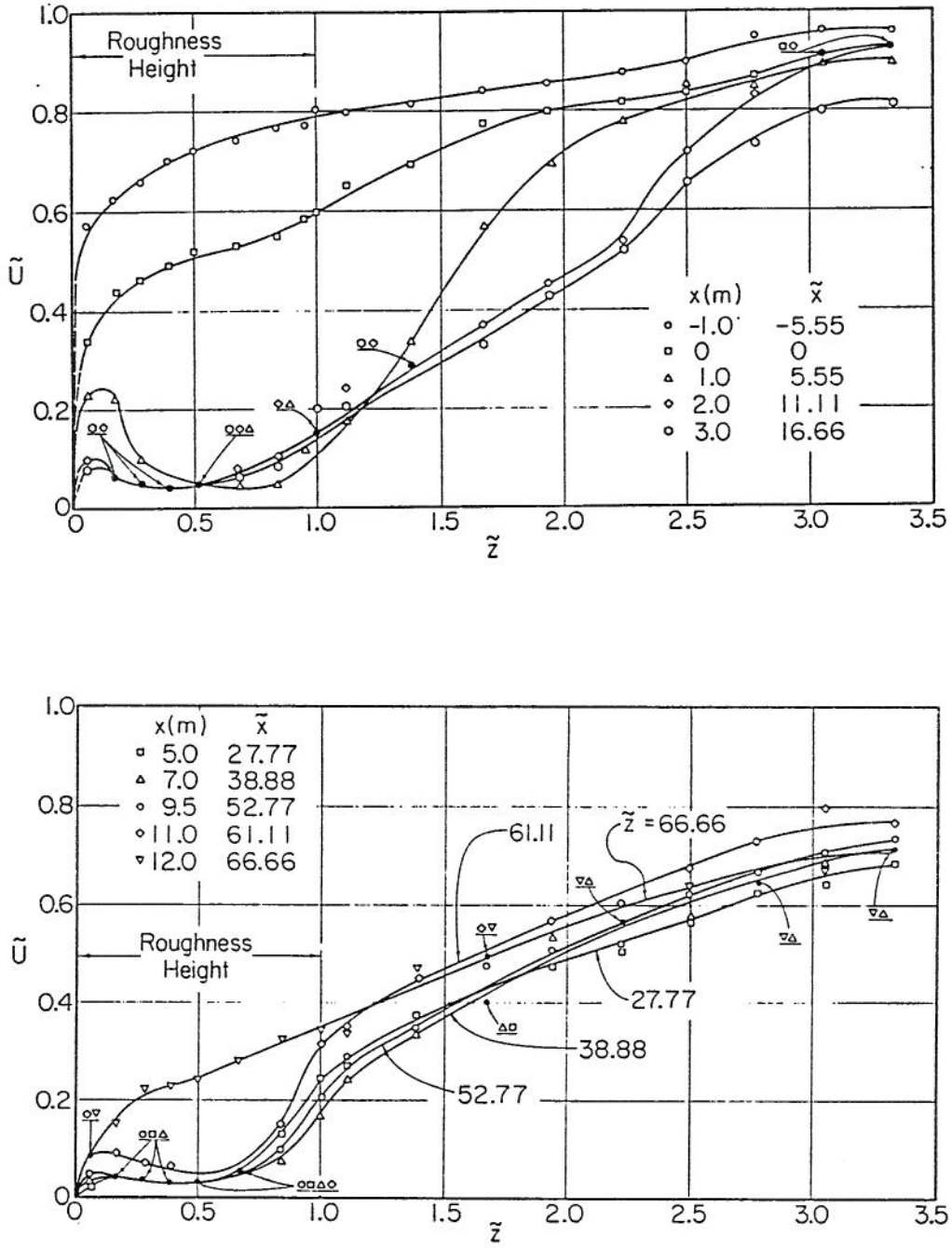


**Figure 3.4.3** Mean velocity profiles within and above the roughness. (Kawatani, 1971)

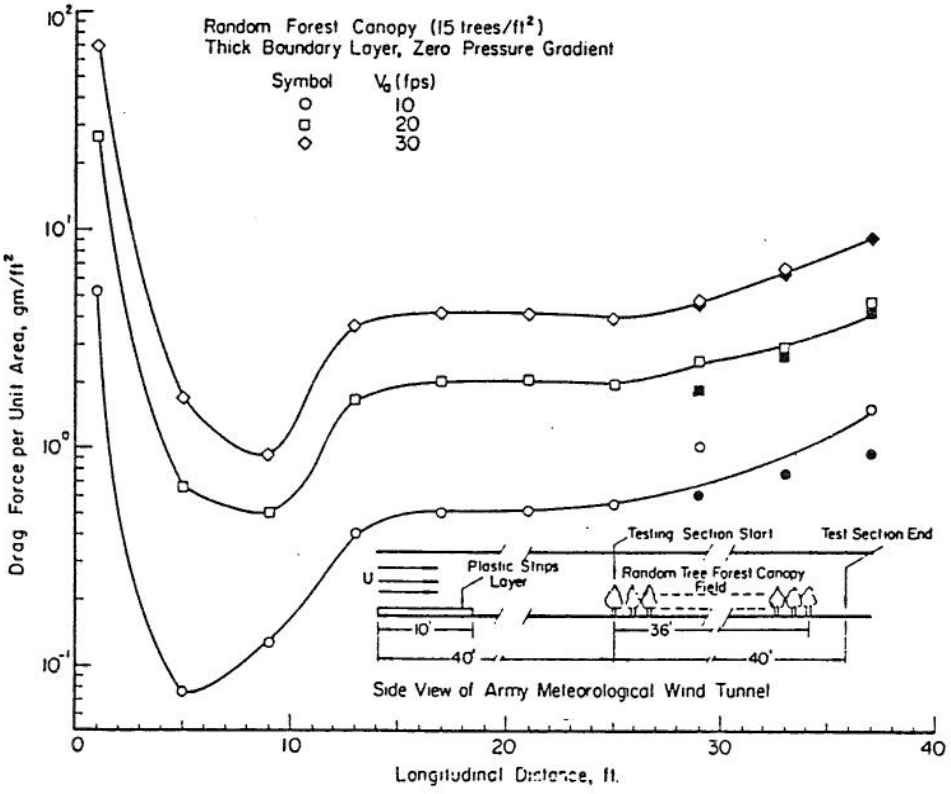


**Figure 3.4.4** Shear plate drag for model forest canopy (Meroney, 1968)

Eimern (1964) considered the aerodynamics of shelterbelts and summarized the influence of density, shape, surface roughness, thermal stratification, wind angle and tree arrangement on downstream wind speed, turbulence, soil moisture, etc.. Simplified insights from this material were incorporated into **Table 3.4.1** by Meroney (1977). Behind porous objects the velocity defect generally persists twice as far downwind; however, the turbulence intensity excess is diminished. Maximum length of shelter will occur for long shelterbelts of near 50% permeability., 30% velocity defect may still exist at 0.5h for $x/h > 50$. The wind will return to its undisturbed condition in about half the distance if the shelter belt is only twice as long as it is high. Wind approaching a shelter belt at an angle increases its effective porosity, decreases the shelter, and increases turbulence excess.

The micrometeorology of shelter belts and forest edges are reviewed by McNaughton (1989). He notes that although extensive studies have been performed downstream of thin shelterbelts the effects of forest edges have received far less attention. Indeed with respect to wind flow downstream of forest edges he notes that "this discussion is more a summary of our ignorance than of our knowledge." There are similarities as well as differences between flow downstream of thin shelterbelts and forest edges. The foliage density of the forest canopy replaces the porosity used for narrow shelterbelts. Upwind profiles must be characterized by the upwind forest roughness, displacement height, forest friction velocity, and foliage density.

McNaughton sought a comparison to the flow over a forest canopy edge and the flow that occurs when a boundary layer passes over a solid backward facing step. For solid steps a recirculating eddy occurs of downwind extent of about 6 h. But permeability often allows the wind to penetrate the forest upwind of the forest edge. For example, wind tunnel experiments performed over plastic model trees (Meroney, 1968) notice winds increased above and within the canopy over the last 10 h. In coniferous forests researchers detect upwind penetration over several heights upwind, but in a denser foliage other researchers see little penetration at all. Nonetheless, little evidence exists to support the presence of a recirculating eddy downwind of the forest edge. The flow velocities and surface shear appear to adjust to the immediate absence of the forest edge by 20 h; however, the wind continues to accelerate over a longer distance as a deeper layer of the atmosphere adjusts to the change of surface roughness.

There appear to be very few measurements of actual winds made above and below forest canopies near clearings or forest edges. Leahey and Hansen (1987) report measurements made on meteorological tower located 60 m from a 0.5 $km^2$ in a forest in Alberta, Canada. Trees were primarily pine and aspen with heights ranging from 18 to 24 m growing on flat terrain. Measurements were taken at 10 and 20 m levels on a 24 m tower using a Gill U-V-W anemometer. They identified strong horizontal jets of air and large vertical velocities during unstable conditions, but rather normal conditions under stable stratification. Winds in excess of 6 $ms^{-1}$ occurred about 15% of the time. Their measurements suggest that clearing a ridge may produce strong convergence toward ridge lines, which could modify ridge top conditions.

**Table 3.4.1** Wake behavior of buildings, trees and shelterbelts (Meroney, 1977)

| DISTANCE DOWNWIND $\frac{X}{H}$ | 5 | | | 10 | | | 20 | | |
|---|---|---|---|---|---|---|---|---|---|
| Flow Variable | $-\Delta V\%$ | $-\Delta P\%$ | T% | $-\Delta V\%$ | $-\Delta P\%$ | T% | $-\Delta V\%$ | $-\Delta P\%$ | T% |
| STRUCTURES (wind directed at face at 90°, measurement at H) | | | | | | | | | |
| W/H = 4 | 36 | 74 | 25 | 14 | 36 | 7 | 5 | 14 | 1 |
| = 3 | 24 | 56 | 15 | 11 | 29 | 5 | 4 | 12 | .5 |
| = 1 | 11 | 29 | 4 | 5 | 14 | 1 | 2 | 6 | - |
| = 0.33 | 2.5 | 7.3 | 2.5 | 1.3 | 4 | .75 | - | - | - |
| = 0.25 | 2.0 | 6. | 2.5 | 1.0 | 3 | .50 | - | - | - |
| INDIVIDUAL TREE | | | | | | | | | |
| Dense Foilage (Colorado Blue Spruce) | 20 | 49 | - | 9 | 17 | - | 4 | 13 | - |
| Thin Foilage (Pines) | 16 | 41 | - | 7 | 18 | - | 3 | 8 | - |
| SHELTER BELTS (Wind measured at - H) | | | | | | | | | |
| Porosity 0% | 40 | 78 | 18 | 15 | 39 | 18 | 3 | 9 | 15 |
| Loose Foilage 20% | 80 | 99 | 9 | 40 | 78 | - | 12 | 32 | - |
| Dense Foilage 40% | 70 | 97 | 34 | 55 | 90 | - | 20 | 49 | - |
| Typical Height of Wake Flow Region | 1.5 | | | 2.0 | | | 3.0 | | |

$$\Delta V\% = \frac{U_o - U}{U_o} \times 100$$

$$\Delta T\% = \frac{\overline{U'}}{U} - \left(\frac{\overline{U'}}{U}\right)_o \times 100$$

$$\Delta P\% = \frac{U^3 - U^3_o}{U^3_o} \times 100$$

Fowler et. al. (1987) examined the effects of shelterwood cutting (30-percent canopy removal) and clearcutting clearings from 0.8 to 8.5 ha on climatic variables of the High Ridge Evaluation Area within the Umatilla National Forest in northeastern Oregon **(Figure 3.4.5).** Areas were harvested in 1976 after nine years of prelogging calibration.

The authors concluded that hydrological effects of the cuttings were surprisingly small, but wind passage and velocities increased dramatically with removal of the forest cover. **Figure 3.4.6** presents data from roughly equivalent 11-month periods during pretreatment and posttreatment. Data presented are for a height of 20 and 6 m above the grounds in watersheds 4 and 1. Little change was noted for the watershed 4, height 20 m case, but at all other locations the wind speeds increased substantially in all classes! One should note that the weather station in watershed 4 was within the uncut area; whereas the station in watershed 1 was in the middle of a clearcut region. Indeed winds at 6 m height in watershed 1 exceeded winds at 20 m height in watershed 4!

Elliott and Barnard (1990a, 1990b) discuss a field experiment to examine the effect of scattered groves of trees and grass on the variability of wind speed and turbulence at the Goodnoe Hills, WA, wind-power site. Two permanent towers and seven portable towers were used. The two permanent towers measured wind at heights from 15 to 107 m and 15 to 59 m above the ground. Wind speed measurements were taken from nine bivane anemometers sampled every second and averaged every minute. The site contains a broad ridge on which the MOD-2 turbines were installed. Terrain is gently sloping to the west and north, but drops abruptly off to the Columbia River Gorge to the south. Vegetation is mostly low sage brush and grass and scattered groves of scrub oak, western juniper and ponderosa pine.

Two towers were about 200-300 m downwind of a grove of 10-18 m high trees at which 20-30 percent reductions of wind speed and a 2-3 times increase in turbulence were measured at a height of 32 m. Wind gusts also increased at 30 m, but by heights of 60 m or distances of 500 m downwind tree effects were considerably reduced (25 to 50 h).

Wind-mill wake and non-wake data sets were created to determine effects of vegetation. Turbulence intensity was defined as the standard deviation of 1-s samples for a 1-min period referenced to a 1-min average speed. The relative arrangement of tree groves and meteorological towers are shown in **Figure 3.4.7**. Towers 6 and 7 evidenced the strongest forest induced wind effects as shown on **Figures 3.4.8 and 3.4.9.** These figures portray the relative wind behavior for different wind directions and associated grove fetch distances. The data set includes situations when the turbines were not operating (NO WAKE) as well as cases when the wind turbine wakes may also interact with the meteorological instruments for some orientations (WAKE). Smaller wake effects are noted for met towers 1, 2, and 9 which are further from the tree stands. Velocities decrease about 10% and turbulence increases no more than 20-30% at these towers.

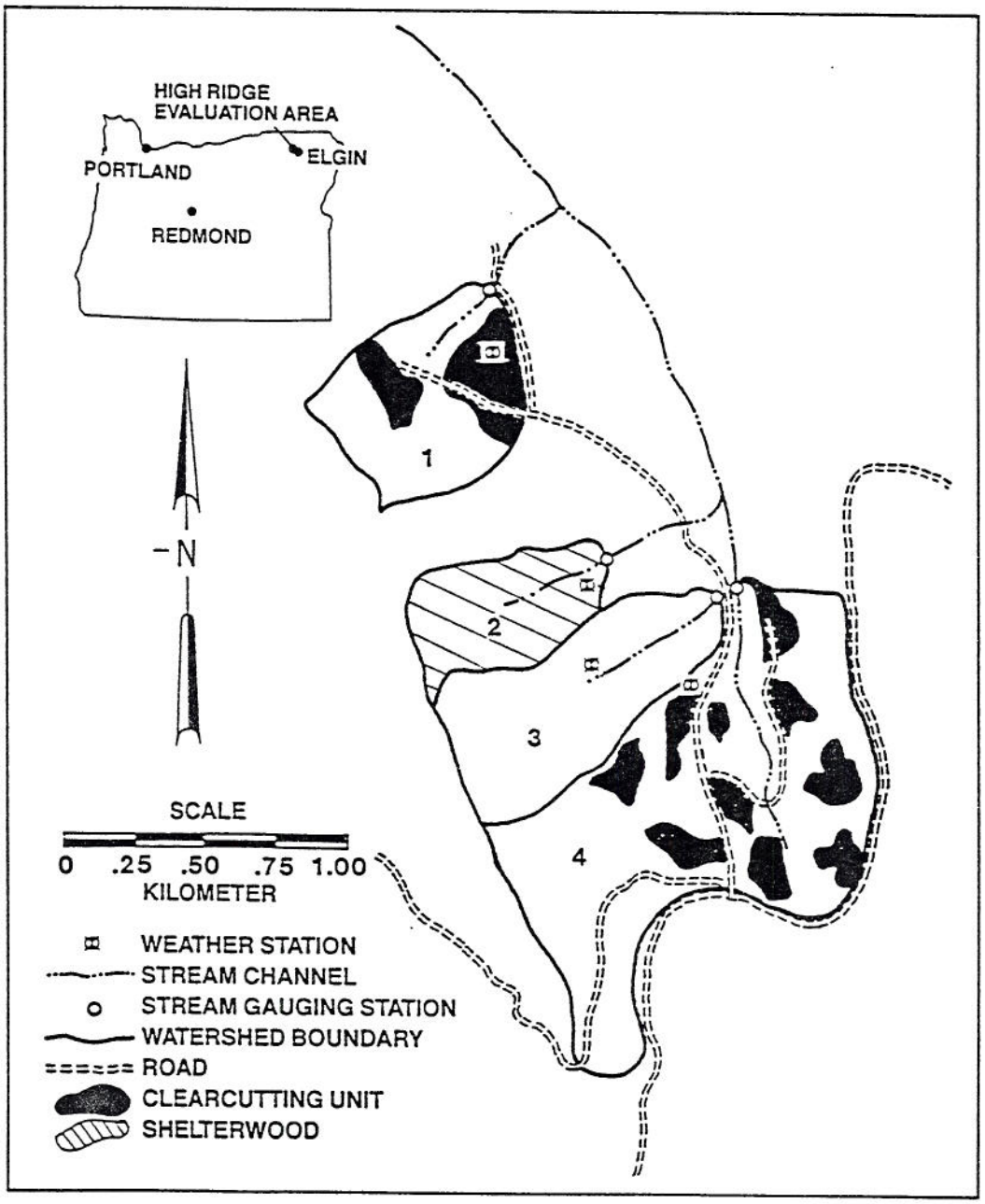


**Figure 3.4.5** Study areas in the High Ridge Evaluation Area, Umatilla National Forest, Oregon. (Fowler, *et al.*, 1987)

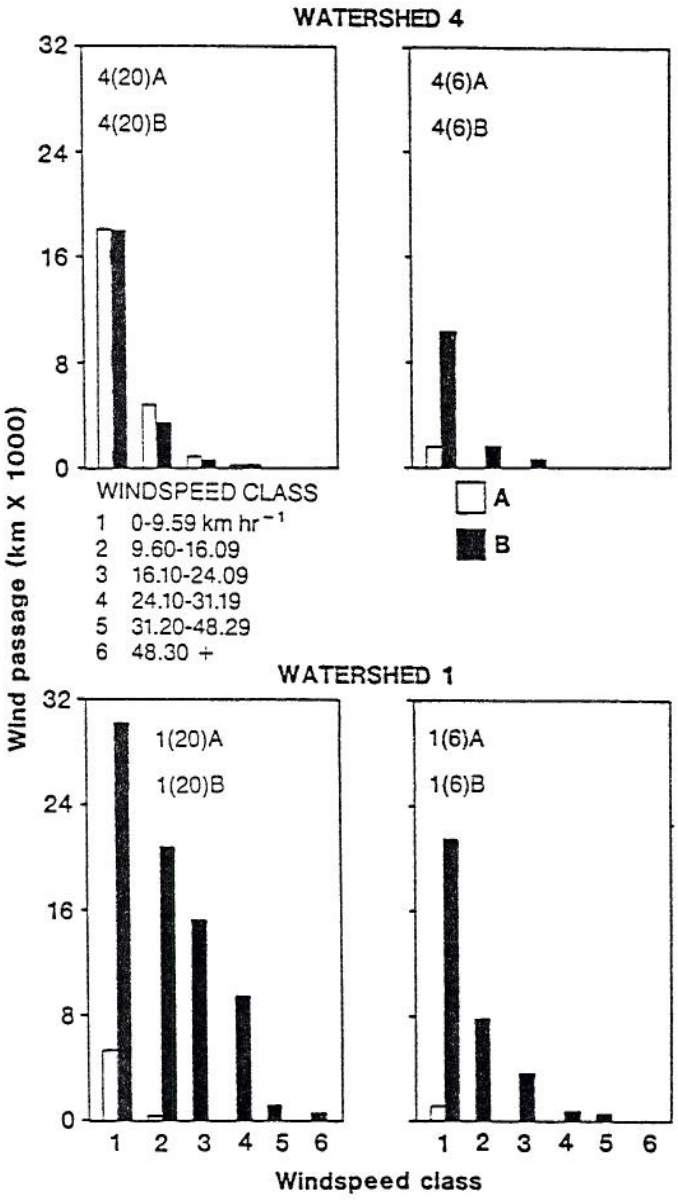


**Figure 3.4.6** Wind passage at 6 and 20m in watersheds 4 and 1 during two 11 month periods--one before and one after treatment. (Fowler *et al.*, 1987)

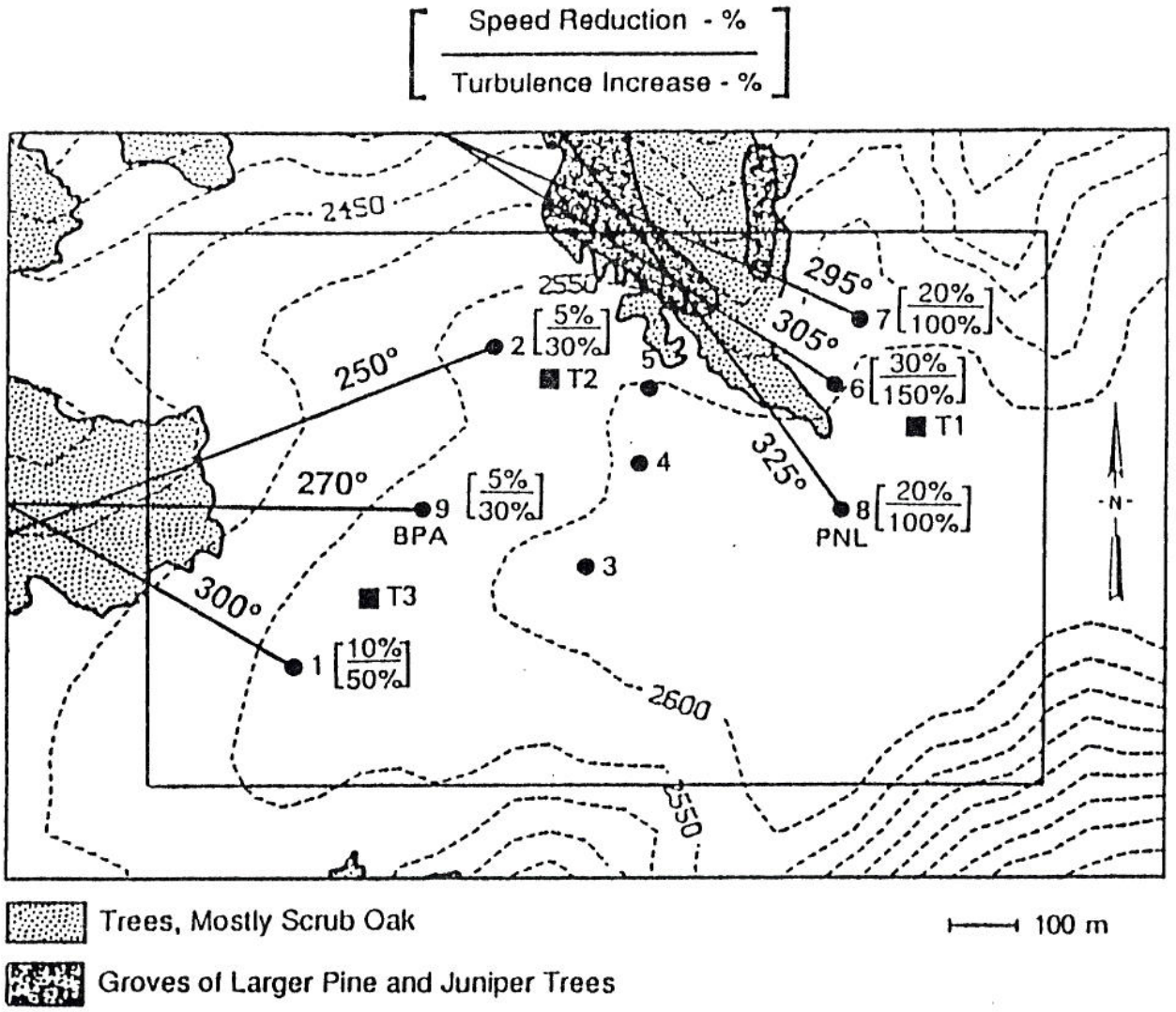


**Figure 3.4.7** Goodnoe Hills, WA. Radials show directions to towers. Percent reduction in wind speed and increase in turbulence [ΔU%/Δu'%] (Elliott and Barnard, 1990)

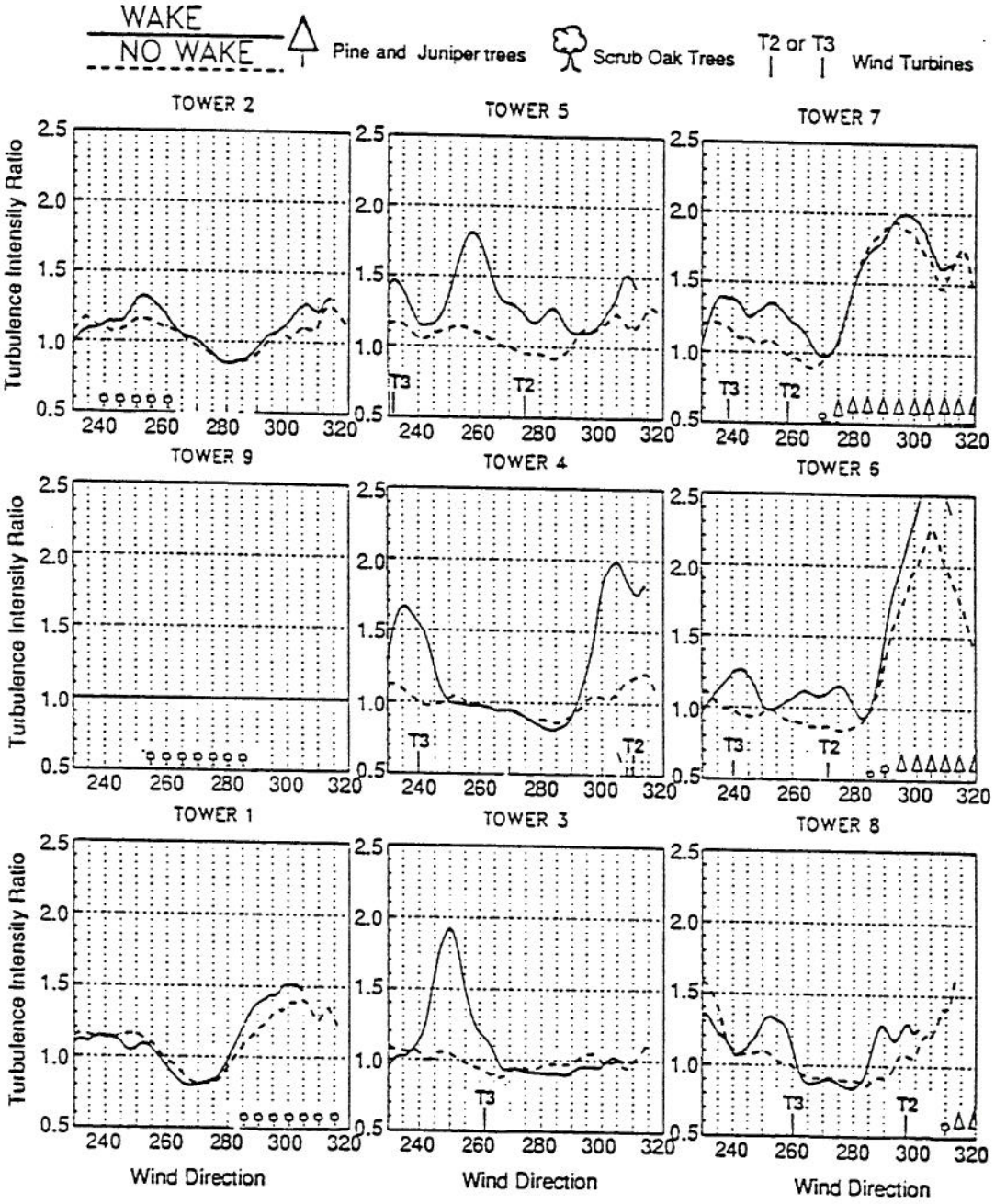


**Figure 3.4.9** Turbulence intensity ratios (to tower 9) versus tower 9 wind direction. (Elliott and Barnard, 1990)

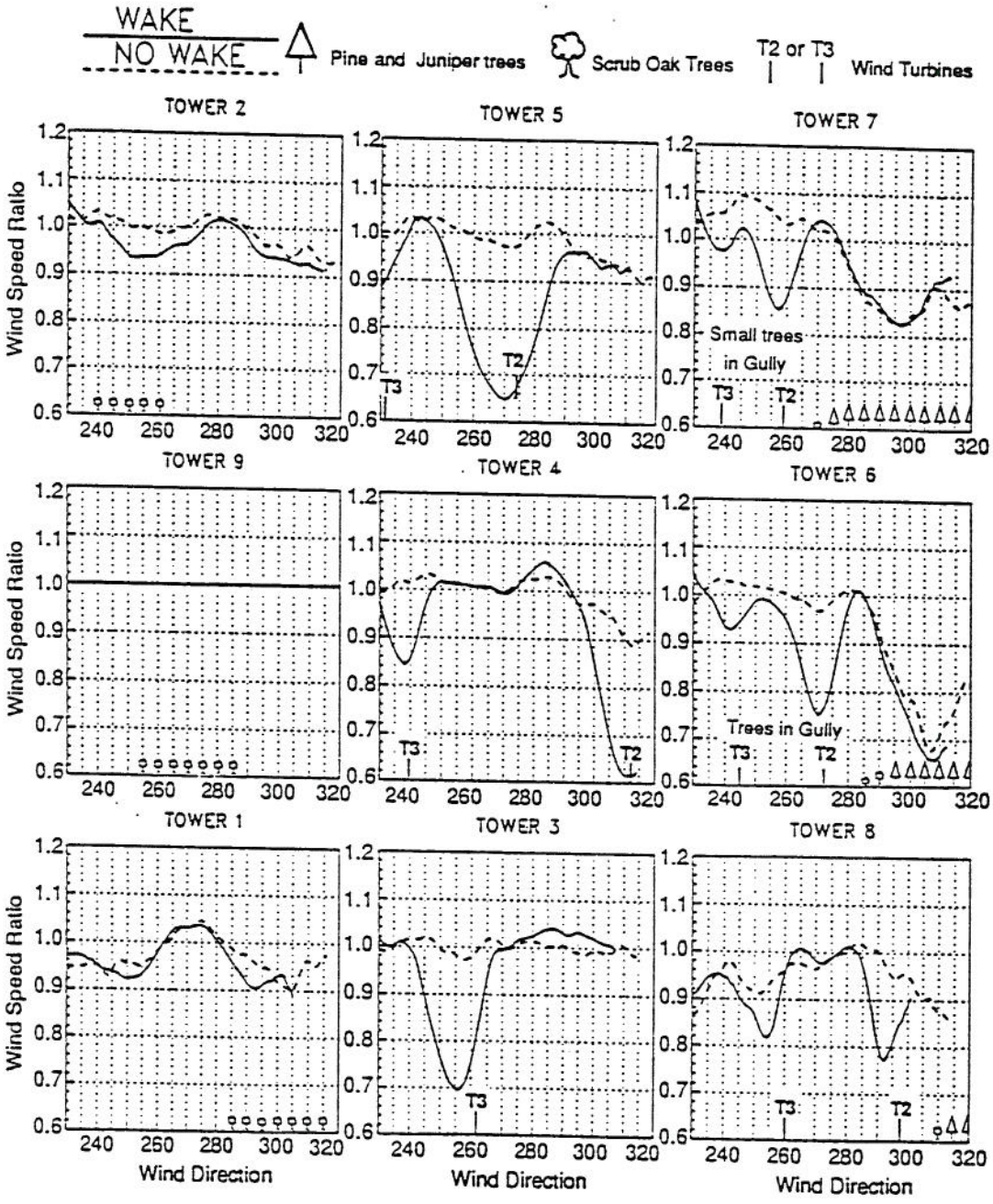


**Figure 3.4.8** Wind speed ratios (to tower 9) versus tower 9 wind direction. Directions of major groves and wind turbines are indicated (Elliott and Barnard, 1990)

The taller towers permitted the authors to examine the effect of height on tree induced perturbations. Winds at the tower within 300 m of groves showed a change of power-law index from 0.14 to 0.28-0.29. The tower at 1000 m showed minimal effects.

## 3.5 Change of Surface Roughness

It has long been observed that when the wind flows from one surface texture to another a transition takes place in wind speed and turbulence within an inner-boundary-layer, $l_z$, that grows in depth with downstream distance from the surface change. When the surface change is associated with roughness height, and downstream wind profiles are plotted semilogarithmically with height, then a distinct "kink" in the slope of the plot is observed which can be associated with this inner-boundary-layer depth, $l_z$. The wind profile near the ground will adjust to surface roughness changes as it moves downwind from the ground cover transition. Above $l_z$ the profiles will correspond to the wind profile for the roughness before the change in cover. Various field measurement programs over smooth-to-rough and rough-to-smooth roughness transitions provide justification for empirical plots of the sort proposed by Park and Schwind (1977). **Figure 3.5.1** consists of five curves that give the growth in transition height between the various profiles of **Figure 3.5.2.** Combining profile shape and transition growth information should permit estimation of a wind speeds below the layer $l_z$ for different downwind distances. The wind speeds above and below the inner boundary layer are adjusted to match at their intersection at $l_z$.

### 3.5.1 *Change of Roughness Models*

A number of different analytic and numerical models exist to predict the resultant variation in wind profiles which exist at different fetch distances downstream of a transition of roughness. The subject is extensive enough that a literature review has been prepared on the topic by Hunt and Simpson (1982). They also provide a table summarizing field and laboratory change of roughness experiments used to verify various models. Unfortunately, little data exists for roughness variations as large as the abrupt change that occurs from a forest edge to a meadow or a clearcut region. Most models grew from the perturbation analysis originally proposed by Townsend (1966). Subsequent researchers have modified assumptions, boundary conditions, definition of perturbation variables and scaling lengths, but the basic concepts have remained the same. This same perturbation approach has subsequently been applied to predicting the effects of surface elevation, surface temperature, surface heating, surface humidity, and stratification on atmospheric boundary layer wind profiles and turbulence.

A presentation by Jensen (1978) is widely accepted. Given an upwind roughness, $z_{o1}$, a downwind roughness, $z_{o2}$, a corresponding up- and downwind surface friction velocity, $u_{*1}$ and $u_{*2}$ , and a distance downwind from the roughness change, x, then:

$$u(x) \approx (u_{*1}/\kappa)\ln[z/z_{o1}] + (u_{*1}/\kappa)\ln[z_{o2}/z_{o1}](\ln[z/z_{o2}]/\ln[l_z/z_{o2}]) - 1\} \quad [3.5.1]$$

$$u_*/u_{*1} \approx 1 + \ln[z_{o2}/z_{o1}]/\ln[l_z/z_{o2}] \quad [3.5.2]$$

$$l_z \ln[l_z/z_{o1}] = 2\,\kappa^2 x \quad [3.5.3]$$

| FROM: \ TO: | A | B | C | D | E | F |
|---|---|---|---|---|---|---|
| A | - | 1 | 1 | 2 | 3 | 4 |
| B | 5 | - | 2 | 3 | 3 | 4 |
| C | 5 | 2 | - | 3 | 4 | 4 |
| D | 5 | 2 | 3 | - | 4 | 5 |
| E | 5 | 3 | 3 | 3 | - | 5 |
| F | 5 | 4 | 4 | 4 | 5 | - |

HOW TO READ THIS PLOT

1) SELECT UPWIND & DOWNWIND TERRAINS IN FIG. 10

2) ENTER TABLE ON LEFT WITH APPROPRIATE LETTERS, SELECT NUMBER

3) USE CURVE BELOW WITH NUMBER

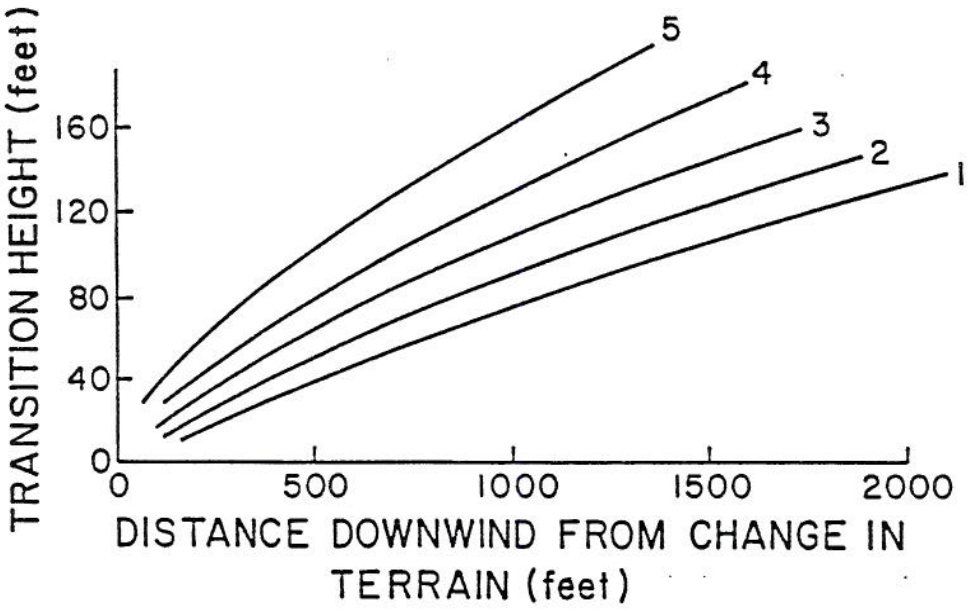


**Figure 3.5.1** Wind profile transition height resulting from a change in surface roughness (Park Schwind, 1977, in Meroney, 1977)

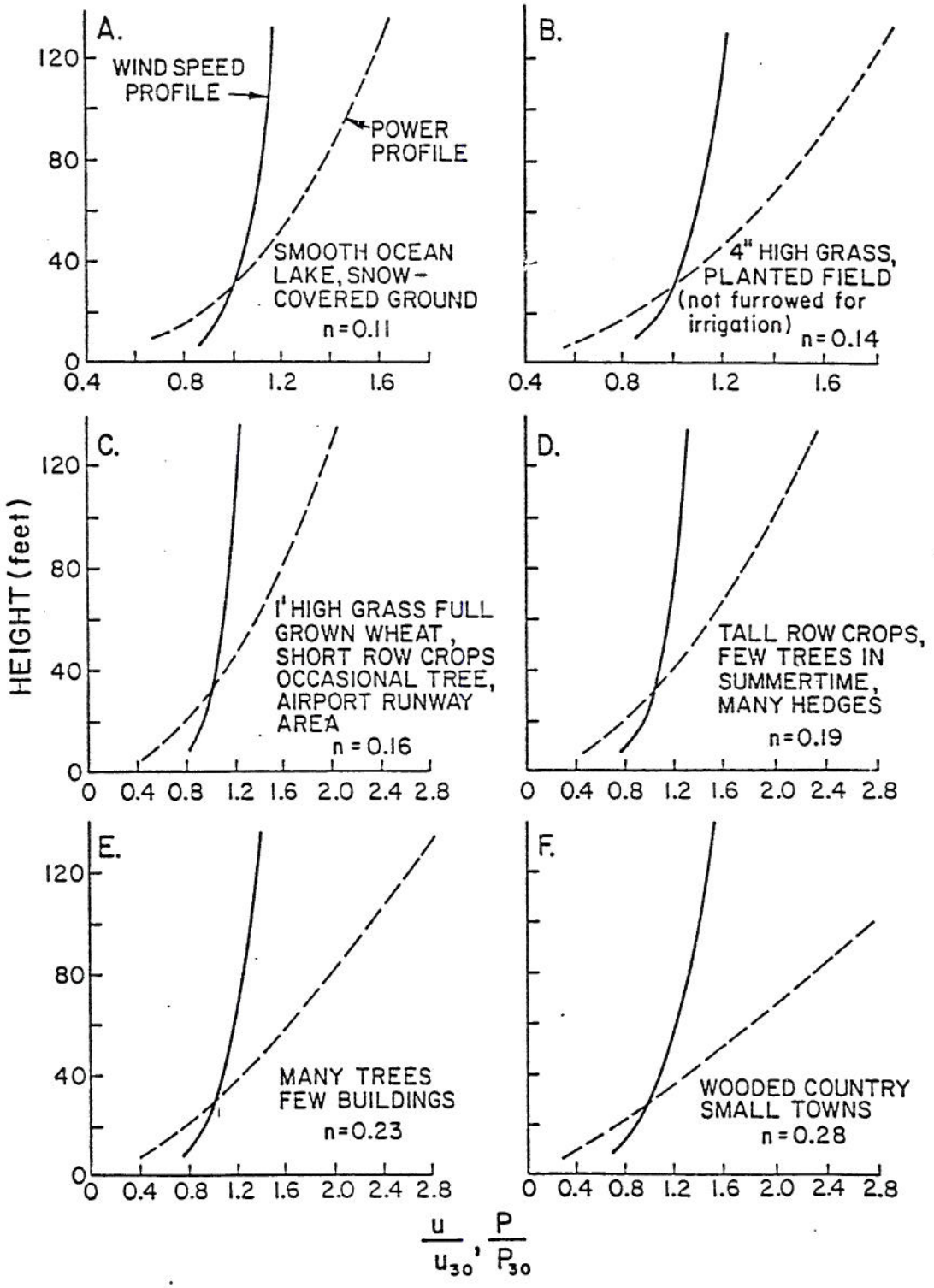


**Figure 3.5.2** Wind profile shapes and wind power profile shapes for various types of flat terrain. (Park and Schwind, 1977)

where $\kappa$ is the von Karman constant commonly set to 0.4. Hunt and Simpson (1982) point out that these expressions suggest that the perturbation shear stress and velocity decrease slowly and inversely with $\ln[l_z / z_{o2}]$ and are proportional to $\ln[z_{o2} / z_{o1}]$. By normalizing $l_z$ and x on the larger of the up- or downwind roughness, $z_o$, an almost universal plot of inner boundary layer growth was prepared from field and model data. As shown in **Figure 3.5.3** the line produced by Equation [3.5.3] is found to lie within 25% of all data. An empirical fit to the nonhomogeneous Equation [3.5.3] might be

$$l_z / z_o = 0.3 \, (x/z_o)^{0.8} \qquad [3.5.4].$$

### 3.5.2 *Multiple changes of roughness*

By superposition of the linear-perturbation solution for a one-dimensional change in surface roughness, one can create a method to predict the effect of arbitrarily distributed surface roughness on wind profiles. Belcher, Xu and Hunt (1990) propose such a model to predict the effect of non-homogeneous two-dimensional roughness on wind profiles and surface stress. Due to the lack of field or model data they compare their results to higher-order turbulence closure solutions of similar boundary conditions. The perturbation approach produces quite good correlation for roughness changes as large as $|\ln[z_{o2} / z_{o1}]|$ of order one.

Derickson and Peterka (1992) have also developed a method to correct anemometers for multiple changes of upwind roughness. Their ad hoc approach follows earlier work on roughness changes proposed by Deaves (1981) and Cook (1985). Whereas the Jensen approach is limited to correcting wind profiles in the lower regions of the boundary layer, this method corrects for the eventual adjustment of the gradient wind profile at all elevations to the change in surface conditions. This method is probably an over-kill for estimating the effects of forest clearings and clearcut regions of finite extent.

## 3.6 Summary

The development of wind profiles over different homogeneous surface roughness conditions can be predicted with fair accuracy. Measured profiles of wind speed both below and above vegetative canopies follow analytic models well. The actual values for surface shear and roughness length will depend upon the total area averaged, especially in areas where surface elevation varies. Surface roughness, $z_o$, and displacement height, d, can be related to canopy foliage density and average tree height. Surface shear can be predicted with somewhat less confidence.

The presence of openings, cleared areas, shelterwood clearings, and clearcut regions within forests produce motions which are qualitatively anticipated. Unfortunately, there are very little field data from forests available to verify any analytic or numerical models for such situations. The downwind effect of roughness change can be predicted by a linear-perturbation model. This model will be used with similar expressions for surface elevation effects to predict the joint effect of nonhomogeneous roughness and elevation in Section 5.4.

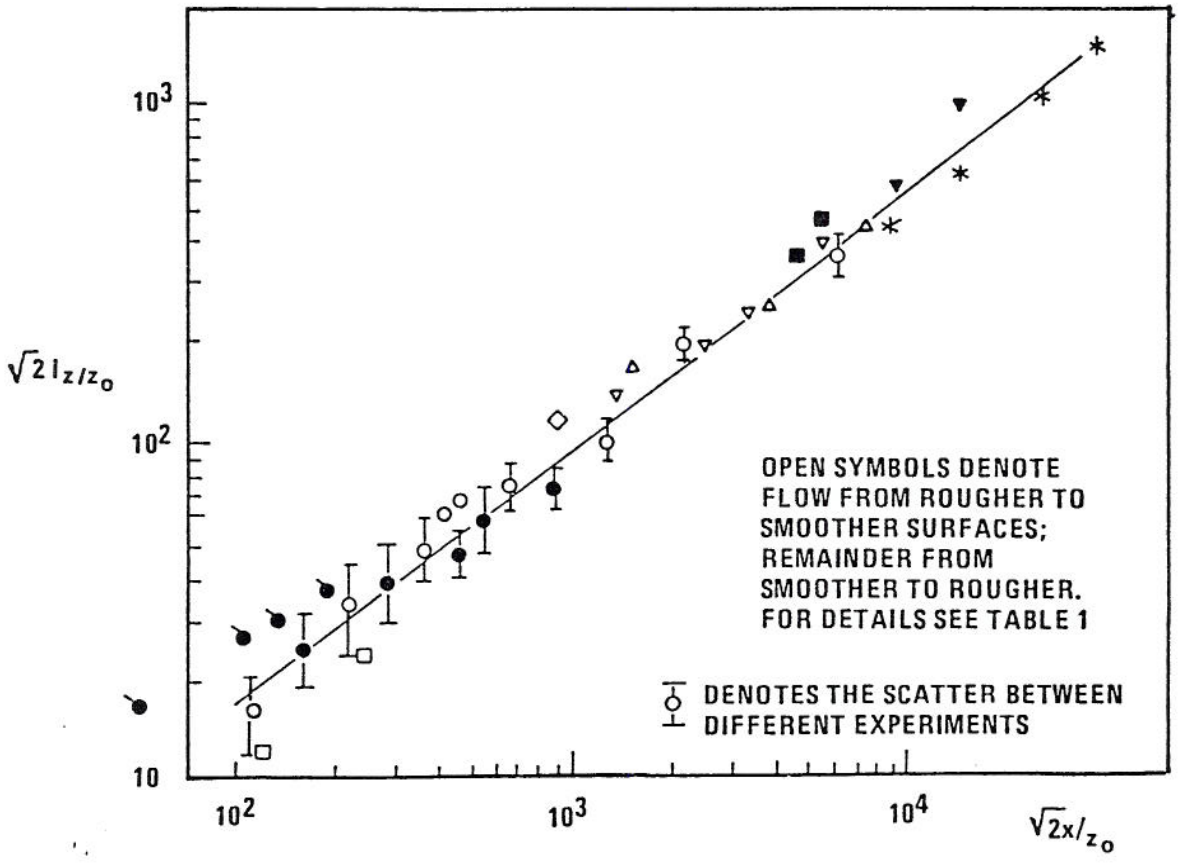


**Figure 3.5.3** Internal boundary layer thickness versus normalized distance referenced to larger $z_o$. Line is best fit to points. (Hunt and Simpson, 1990)

# IV. VEGETATIVE/SURFACE ROUGHNESS EFFECTS ON FLOW OVER HILLS /MOUNTAINS

Complex hilly terrain may exist with a variety of vegetative surface cover. For example the approach terrain and the hill itself may both be either bare or vegetation covered. Alternatively, the upwind surface may be smooth (farmed plains or meadows) and the hills may be rough (tree covered), or the upwind surface may be rough (tree covered) and the hill itself bare. In some cases only portions of the hill may be bare due to selective shelterwood cutting or clearcutting. The presence or absence of high roughness may lead to lower/higher wind speeds, higher/lower turbulence, or attached/separated streamline flow.

## 4.1 Homogeneous Surface Roughness Over Hills/Mountains

The upwind surface roughness induces different approach velocity profiles which can lead to variations in hill crest wind profiles **(Figure 4.1.1).** The approximate effects of such profile changes on the fractional speedup have been examined using physical modeling, inviscid rotational numerical models, 2nd-order turbulent closure models and linear-perturbation analysis.

### 4.1.1 *Field and Laboratory Data*

Bouwmeester et al. (1978) performed wind tunnel measurements over triangular hill shapes, with equal hill heights and slope, but surface roughness varying between cases by a factor of ten ($z_o/h_{hill}$ = 0.0013 versus 0.0178). The measured values of fractional speedup, $\Delta S$, for smooth and rough hills are plotted in **Figure 4.1.2** as Test Case 5 and 14, respectively. The rough hill produced larger speedup values at all heights; however, since the reference wind speed at a given height is usually less for rough surface flows, the actual crest height wind speeds are less. Additional smooth surfaced hill measurements are also plotted for other hill slopes as Test Cases, I, 3 and 9.

In Section 2.2 it was noted that Bradley (1978) measured wind flows over a tree-covered ridge in Australia. The ridge height, $h_{hill}$, was 170m, the upwind ridge length was $L_u$ = 550 m and the downwind length somewhat longer, $L_d$ = 600 m.; hence, the average $h_{hill}$ /L ratio equals about 0.29. The hill was covered with 10 m tall trees, and the associated surface roughness, $z_o$, and displacement height, d, were estimated to be 1.0 m and 7.0 m respectively; hence, $z_o/h_{hill}$ = 0.006. The atmospheric boundary layer was estimated to be between 600 and 800 m. Bradley obtained wind data at various heights up to 100 m above the crest during neutral conditions. A separation region was believed to exist downwind of the crest. The fractional speedup for this hill is also plotted on **Figure 4.1.2.** where vertical heights have been correct for forest displacement above the ridge ground level. The roughened wind-tunnel model was relatively slightly rougher than the Bradley forested hill. Note that the inner-boundary-layer, $l_z$ is noticeable at a dimensionless height of about 0.17. The magnitude of $l_z$ during the model tests was believed to be considerably smaller than this due to relaminarization at low Reynolds numbers.

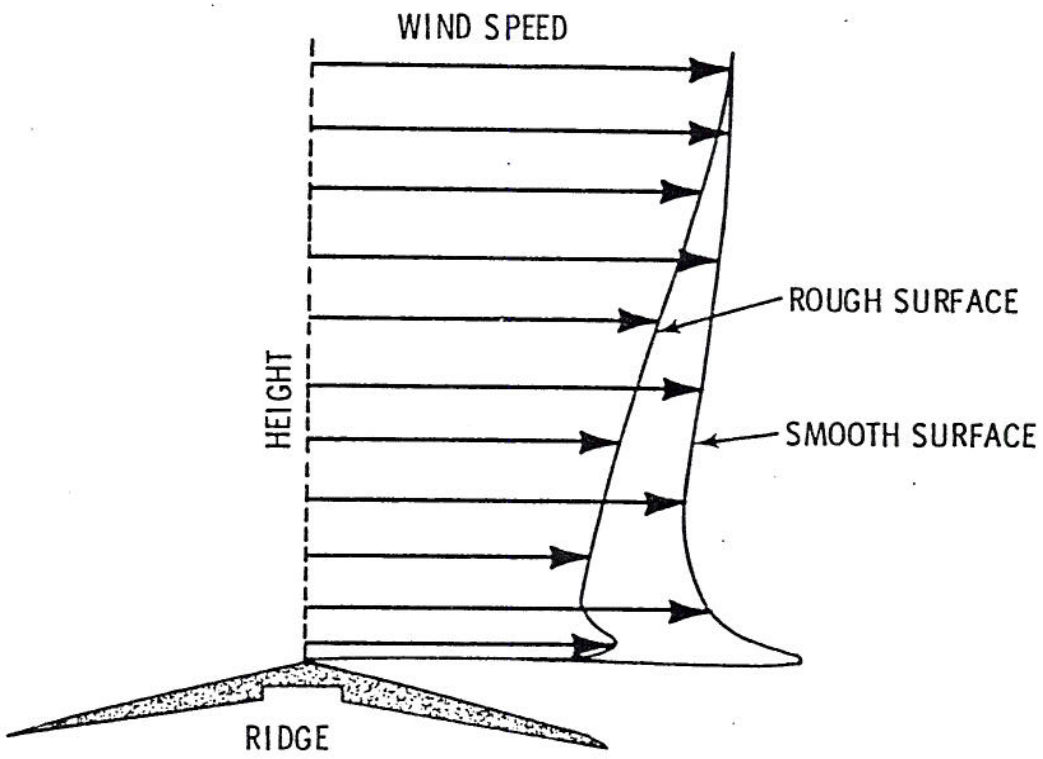


**Figure 4.1.1** Effect of surface roughness on wind flow over a sharp-crested ridge. (Wegley, Orgill and Drake, 1978)

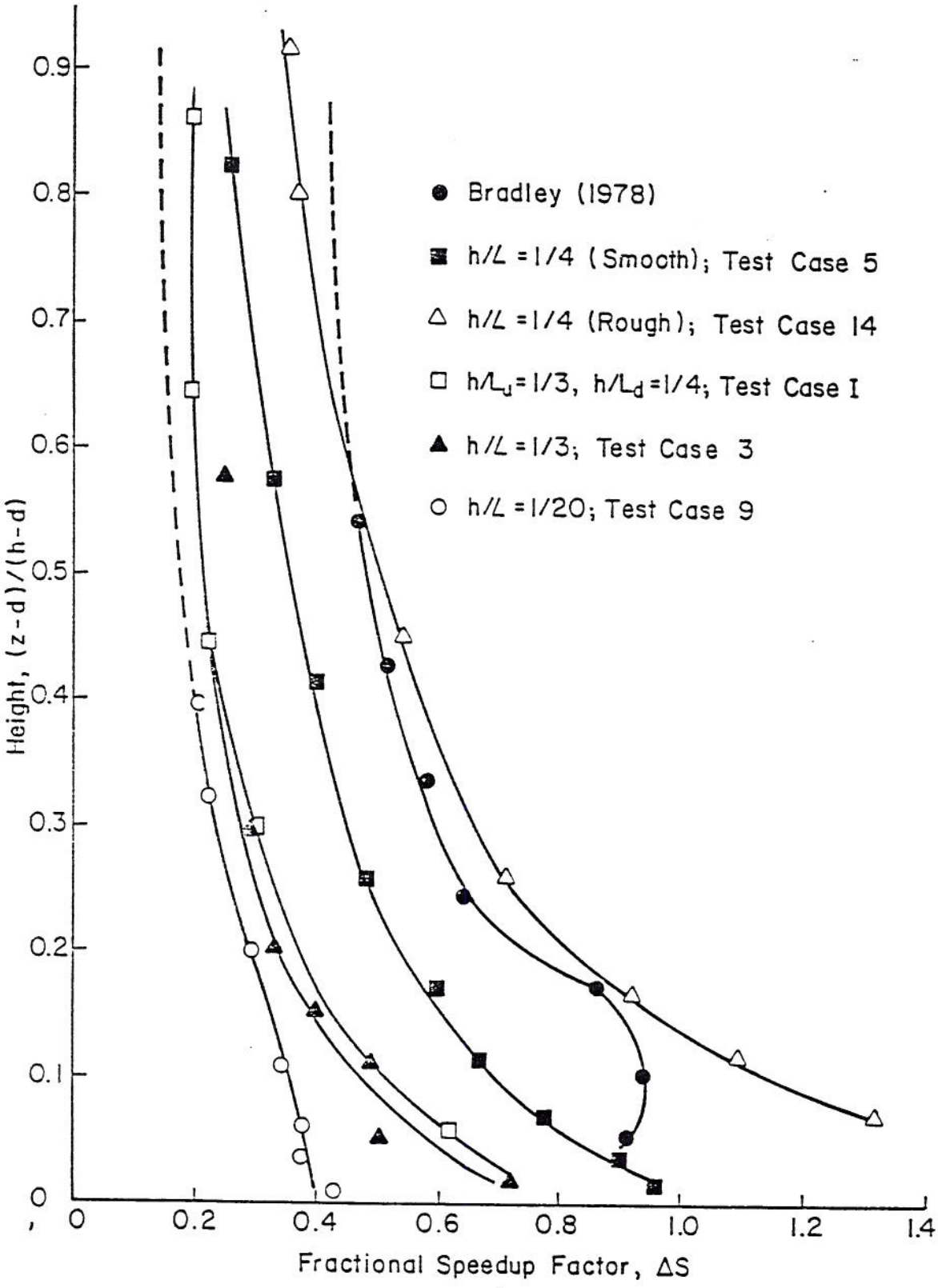


**Figure 4.1.2** Fractional speedup ratio profiles at crest of triangular hills. Field data,Bradley (1978); Laboratory data, Bouwmeester *et al.* (1978)

### 4.1.2 *Inviscid -Rotational Numerical Model Results*

Bouwmeester et al. (1978) used the inviscid-rotational potential flow model proposed by Derickson and Meroney (1977) to predict fractional wind speed up over hills for different approach flow profiles. In **Figure 4.1.3** nine velocity distributions are plotted for different combinations of $z_o/h_{hill}$ and $h_{hill}/\delta$. Resultant fractional speedup ratios, $\Delta S$, are shown in **Figure 4.1.4.** The fractional speedup ratios are essentially independent of roughness for $h_{hill}/\delta = 4$, and there is only a slight dependency on roughness for smaller $h_{hill}/\delta$ values. The upper flow perturbations proposed by Jackson and Hunt (1975) are also essentially inviscid potential flow solutions, and they also imply primary dependence on hill slope and no variation with surface roughness, that is $\Delta S = (h_{hill}/L)\sigma(x,y)$. These results seem inconsistent with the measurements reported in Section 4.1.1. One reason might be that despite the range of roughnesses specified for the upwind profiles, the absolute roughness magnitudes were less than $z_o/h_{hill} = 10^{-4}$. The differences might also result because the inviscid model does not correct for the inner-boundary layer which increases as $l_{z1}/l_{z2} = (z_{o1}/z_{o2})^{0.2}$ . Thus, if the roughness length increases by a factor of ten the inner-boundary-layer increases by almost two..

### 4.1.3 *Turbulence Model Insights*

Frost, Maus and Fichtl (1974) solved the turbulent boundary layer equations over a plane surface using mixing-length closure for a horizontal pressure distribution equal to that along the $\psi = 0.6$ streamline of inviscid potential flow around an elliptical cylinder. Numerical solutions were carried out for aspect ratios 2:1 and 4:1 and for various surface roughness lengths. **Figure 4.1.5** shows the resulting wind profile directly over the crest of the ellipse with alternate roughness lengths and aspect ratios. Notice that the inner-boundary-layer length, $l_z$ (or in this case shown as $\delta$) increases with larger roughness such that $\delta_1/\delta_2 \approx 1.33$, which agrees well with the value $(z_{o1}/z_{o2})^{0.2} = 1.38$ suggested by manipulation of Equation [3.5.4]. Fractional speed up at inner-boundary-layer height appears to remain nearly constant as roughness increases.

Taylor and Gent (1974) solved for flow over a hypothetical hill using second-order turbulence closure methods. Bouwmeester et al. (1978) determined that surface shear stress predicted by inviscid models underestimated the Taylor-Gent nonlinear model values by up to 300%.

### 4.1.4 *Linear-perturbation Model Insights*

Linear-perturbation models of the sort used by Jackson and Hunt (1975), Jensen (1978), and Jensen and Petersen (1978) provide for the influence of surface roughness in an inner layer, $l_z$, such that the fractional speed up becomes:

$$\Delta S(z) = (h_{hill}/L)\sigma(x)\,(\ln[L/z_o]/\ln[l_z/z_o])^2, \qquad [4.1.1]$$

where $\sigma(x)$ adjusts for dimensionless hill shape, f(x/L). The factor is maximum at hill crest, $\sigma_{max} \approx \sigma(0) = \Delta u_{max}/[(h_{hill}/L)u_o]$. Typical values of $\sigma_{max}$ are displayed in **Table 4.1.4 .**